J. Condensed Matter Nucl. Sci. 13 (2014) 277–289

Research Article

Recent Progress in Gas-phase Hydrogen Isotope Absorption/Adsorption Experiments

A. Kitamura *†, Y. Miyoshi, H. Sakoh, A. Taniike and Y. Furuyama
Graduate School of Maritime Sciences, Kobe University, Kobe 6580022, Japan

A. Takahashi ‡, R. Seto and Y. Fujita
Technova Inc., Tokyo 1000011, Japan

T. Murota and T. Tahara
Santoku Corp., Kobe 6580013, Japan

Abstract

To enhance reusability of the nanopowder samples for heat generation by gas-phase hydrogen isotope absorption, porous-silica-inclusion has been applied to Pd nanopowders (PSII) and Pd·Ni nanocomposite (PNS) samples. Absorption parameters repeatedly obtained in the repeated runs including repeated oxidization-hydridation cycles suggest interesting role of admixed minority atoms in the nanoparticles.
 ISSN 2227-3123

Keywords: Hydrogen isotope absorption, Inclusion, Nanoporous-silica, Pd nanoparticles

1. Introduction

Gas-phase hydrogen isotope absorption/adsorption experiments have been performed since 2008 at Kobe University to elucidate the mechanism of anomalously large heat release. The samples include 0.1-μm-diam. Pd particles (PP, Nilaco Corp.), Pd-black (PB, Nilaco Corp.), oxide nanocomposites of Pd·ZrO_2 (PZ, Santoku Corp.), ternary oxide compound of Pd·Ni·ZrO_2 (PNZ, Santoku Corp.), binary oxide compound of Ni·ZrO_2 (NZ, Santoku Corp.), Pd·Ni nanoparticles dispersed in ZrO_2 powders provided by B. Ahern (PNZ2B), and porous-silica-included Pd nanoparticles (PSII, Admatechs Co. Ltd.).

*E-mail: kitamuraakira3@gmail.com
†Also at: Technova Inc, Tokyo 1000011, Japan
‡Also at: Osaka University, Suita 5650871, Japan

 ISSN 2227-3123

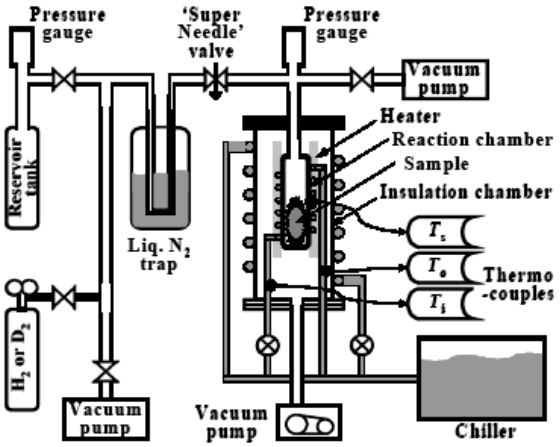

Figure 1. Schematic of one-part of the twin system.

Based on the results of the extended measurements, the effects of the sample structure on the absorption/adsorption characteristics have been discussed; particle size, oxide formation on the Pd samples, the silica-inclusion of Pd nanoparticles, and Ni-substitution for Pd. Anomalously large values of the evolved heat, the total D/Pd (H/Pd) loading ratios and the η-values have been repeatedly observed in the absorption runs at room temperature using the samples of PZ [1–3], PSII [4] and PNZ2B [5]. It has been found that addition of a small amount of Pd to the Ni nanoparticle sample changes the absorption characteristics of Ni drastically to enhance the loading ratio and heat release [5].

These results have prompted examination of two kinds of the sample; ternary oxide compound of Cu·Ni·ZrO_2 (CNZ, Santoku Corp.) and porous-silica-included Pd·Ni nanoparticles (PNS, Admatechs Co. Ltd.).

The CNZ sample was fabricated for the purpose of checking whether Cu atoms can substitute for Pd atoms in the PNZ2B sample. Preliminary results show that the CNZ sample requires elevated temperature to absorb hydrogen isotopes. Slight and long-term increase in temperature have been observed in some runs operated at above 500 K. Detailed description of the experiments using this sample is given in another presentation by H. Sakoh [6] in this Conference.

In the present paper the characteristics of the nanoporous-SiO_2-included samples, PSII and PNS, are discussed in detail. It is well known that Pd nanoparticles clump together to become agglomerated, when simple nanoparticle samples of Pd are subjected to repeated use for gas-phase hydrogen isotope absorption experiments. This causes substantial decrease in absorbed amount of hydrogen isotopes and induced heat release for the second use or more.

It has been reported that large heat release with isotopic difference was observed under hydrogen isotope absorption by Pd nanopowders included in the basket structure of zeolite [7]. Purpose of inclusion in the basket structure is to prevent agglomeration of nanoparticles of Pd under repeated use. In the present study we have used nanoporous-silica-included Pd (PSII) or Pd·Ni (PNS) nanoparticles manufactured by Admatechs Co., Ltd. instead of zeolite-included one to study effect of such structure on absorption and heat release characteristics. The latter PNS sample was fabricated to have a mixture of Pd and Ni with a molar fraction of about 0.01 and 0.06, respectively, in expectation of the similar function of the Pd atoms in the PNZ2B sample.

2. Experimental Apparatus and Procedure

The PSII sample is composed of nanoparticles of Pd and nanoporous-silica with a mean size of 4 μm. The size of Pd ranges from about 3 nm to about 150 nm, with 90% being 3–10 nm.

We have used a twin absorption system consisting of two equivalent chambers for hydrogen isotope gas absorption/adsorption experiments. Figure 1 shows a schematic of one-part of the twin system. The samples are put in the reaction chamber, and the outer chamber is evacuated for thermal insulation during hydrogen isotope absorption/adsorption. Sheath heaters with resistance of 37.9 and 53.8 Ω wound around the reaction chambers in the A_1 and A_2 systems, respectively, are used for sample heating in the cases of baking, forced deoxidization, forced oxidization and absorption runs at elevated temperatures. Alumel-chromel thermo-couples are used to measure temperatures.

For the PSII samples, mass flow calorimetry was employed. The coolant water temperature is maintained constant (±0.1°C) at near-room temperature with a chiller, and the flow rate is controlled with a digital coolant transmitter at a rate of 12 cm^3/min, which recovers heat with an efficiency of 90.0±1.7%. Calorific power is calculated from temperature difference between the exit and the entrance of water-coolant. There is a delay in the response of the temperature difference due to the indicial response with a time constant of 2.2 min. The calibrated conversion factor is 0.929 W/K.

On the other hand, since we expected that the PNS sample exhibits better performance at elevated temperatures [8], the power measurement in the PNS absorption runs were performed by isothermal calorimetry. In this case, water was taken out of the coolant pipe, and the output power was deduced from the relation between the temperature of the reaction chamber wall and the thermal power. The thermocouples were rearranged to measure the temperatures of the surface of the reaction chamber at the bottom, the side and the top.

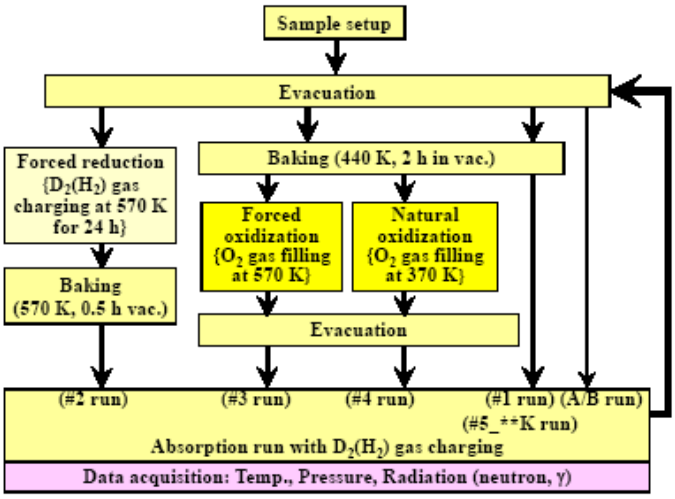

Figure 2. Flowchart of the experimental procedure.

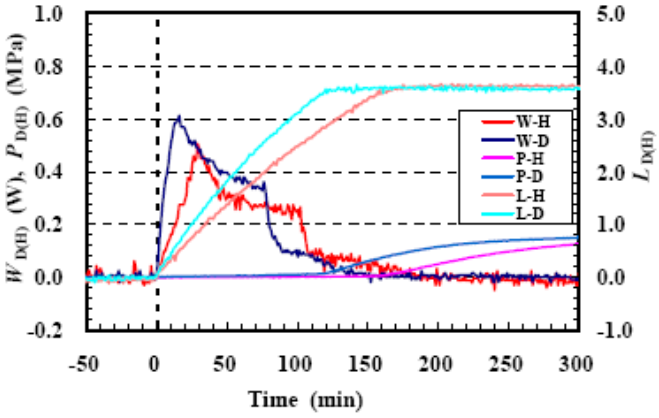

Figure 3. Evolution of thermal power $W_{D(H)}$, pressure $P_{D(H)}$ in the reaction chamber after introduction of D_2 (or H_2) gas and the time-dependent loading ratio $L_{D(H)}$ in runs D-PSII3#1 and H-PSII4#1.

This relation was obtained beforehand in the calibration runs using the power supplied to the heater, and is shown in Table 2 of ref. [6]. The conversion factor to the power depends on temperature, and is 0.16 W/K at room temperature, and about 1.0 W/K at 573 K.

Since the major path for the heat loss is absent, the time constant becomes much longer than in the case of the mass-flow calorimetry. It was measured in the above calibration using a stepwise variation of the heater power to reveal two components in the temperature decay curve with time constant of 16 and 45 min due to radiation and conduction, respectively.

Figure 2 shows the experimental procedure. The run number expresses the conditions of the sample used in the run, using the letters defined in Table 1. The as-received sample is baked at 440 K for 2 h in vacuum, and subjected to the D_2 (H_2) absorption run (#1 run). The sample is reused either without any treatment (A or B run) or after the specified treatment; forced deoxidization (#2 run) or forced oxidization (#3 run) or passive oxidization (#4 run). For Ni-based samples, NZ, CNZ and PNS, high temperature was required for appreciable absorption of hydrogen. The run at an elevated temperature of T K is called "#n_TK" run.

The detailed descriptions of the run procedures are found in other papers; e.g., [4] for the room-temperature runs with mass flow calorimetry, and [6] for the high-temperature runs with isothermal calorimetry.

Table 1. Nomenclature for the run number.

#1	Absorption run using a virgin sample
#2	Absorption run after forced de-oxidization
#3	Absorption run after forced oxidization
#4	Absorption run after natural oxidization
#nA	Absorption run following #n without baking
#nB	Absorption run following #nA without baking
#n(N)d	Desorption run by evacuation after an absorption run #n(N)
#5_TK	Absorption run at an elevated temperature of T K

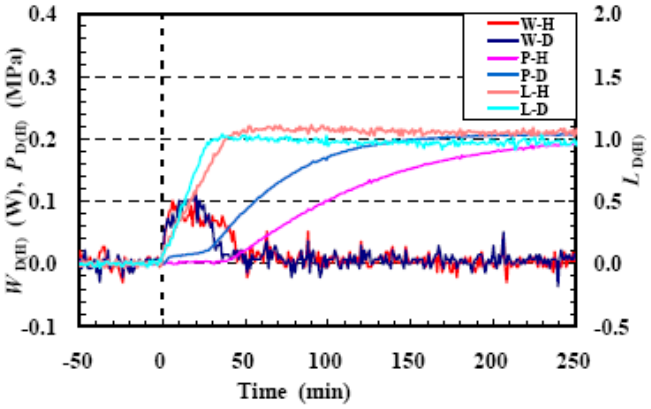

Figure 4. The runs after forced deoxidization, D-PSII1#2 and H-PSII2#2.

3. Results and Discussion

3.1. PSII sample

First we discuss the effect of silica inclusion of the Pd nanopowders. Figure 3 shows typical variation of the heat output, $W_D(t)$ and $W_H(t)$, pressure in the reaction chamber, $P_D(t)$ and $P_H(t)$, and the loading ratio, $L_D(t)$ and $L_H(t)$, in the hydrogen isotope absorption run for ten-gram aliquots of as-received samples, D-PSII3 and H-PSII4, respectively. The D(H)-PSII3(4)#1 runs have extraordinary large loading ratios $L_{D(H)}(t)$ which reach D(H)/Pd $\approx$ 3.6 (3.5) at the end of the exothermic phase. This phase is thought to be dominated by chemical process, and is called the first phase in the present work. The 1st phase involves processes of surface adsorption, oxygen pickup reaction and absorption into the bulk. Contributions of these processes to the time-dependent parameters, $W_{D(H)}(t)$ and $L_{D(H)}(t)$, and their time-integrated parameters, $E_{1D(H)}$ and D(H)/Pd, are discussed later in this paper.

The specific heat release $E_{1D(H)}$ is also very large; $E_1 \approx 2.7$ (2.4) eV/atom-Pd for D(H). The values of the loading ratio are more than 4 times larger than the maximum value of 0.85 ever observed for loading bulk Pd metal, while the values of the specific heat release evaluated as the energy per one D(H) atom absorption give 0.75 (0.69) eV/atom-D(H), which is also about 4 times larger than the value of 0.2 eV/atom-H for the bulk-Pd metal, and even a factor of 1.5 (1.4) larger when compared with the surface adsorption energy of 0.5 eV/atom-H for bulk-Pd metal.

After finishing the #1 run, we made forced deoxidization at 573 K. Figure 4 shows the #2 absorption runs using these samples. The values of D(H)/Pd and E_1 were 0.95 (1.02) and 0.21 eV/atom-Pd, respectively. The loading ratio is slightly larger than that for the bulk Pd, and the values of the released heat give 0.22 (0.20) eV/atom-D(H) which are nearly equal to the bulk value. It appears that the deoxidized samples have fewer adsorption sites, and/or very small adsorption energy. If the former is the case, a higher temperature and/or a longer period of heating are/is necessary in the deoxidizing process for purging the D(H) atoms in the adsorption sites on the PSII sample surface.

Forced oxidization of the samples was performed by keeping them in the O_2 atmosphere at a temperature of 570 K for 30 h. The degree of oxidization, x ($\equiv$ PdO/Pd), is calculated from the pressure difference between the beginning (0.3 MPa) and the end of the exposure to O_2 in the closed system. The values of x ranged from 0.69 to 0.79. Figure 5 shows the traces of the parameters in the #3 absorption runs using the oxidized samples. The oxidized samples has almost recovered the large values of E_1 and D(H)/Pd.

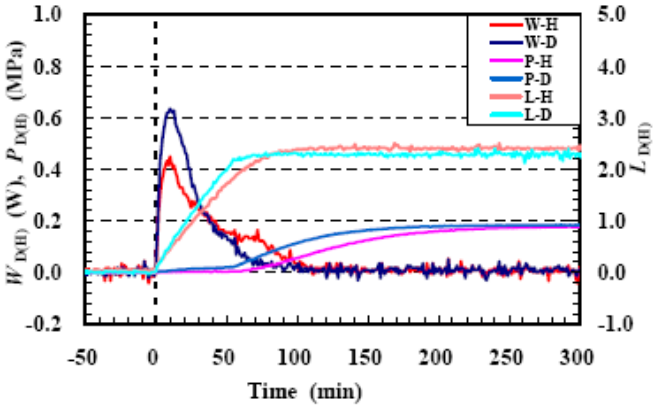

Figure 5. The absorption runs after forced oxidization, D-PSII3#3_3 and H-PSII4#3_3.

Next, the samples were left outside the chamber for 24 h to allow natural oxidization in the ambient air, and subjected to the #4 absorption runs. Then the samples were subjected to forced oxidization again, followed by #3_2 absorption runs, which were also followed by passive oxidization runs twice, #4_2 and #4_3.

Figures 6 and 7 show the parameters E_1 and D(H)/Pd, respectively, for runs #1 through #4_3 as histograms. In the PSII#1 run the released heat and the loading ratio were both considerably large in comparison with the bulk Pd as described above. The loading ratios of the A, B and #2 runs were about 1.0 and slightly larger than that of the bulk Pd, while the released heat remained the bulk value. In the two runs after the forced oxidization of the samples, #3 and #3_2, the released heat and the loading ratio were largely recovered. However, the passive oxidization was not effective for substantial recovery of the large values of the loading ratio and the released heat.

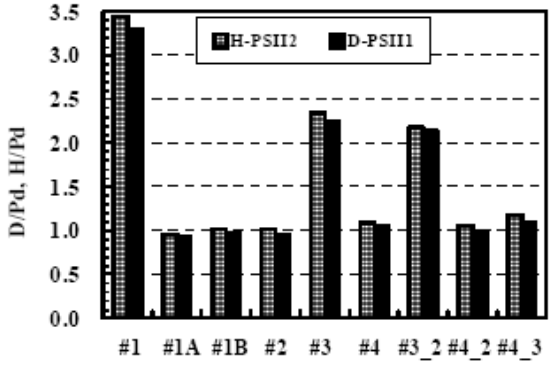

Figure 6. Specific heat release E_1 for the samples D-PSII1 and H-PSII2.

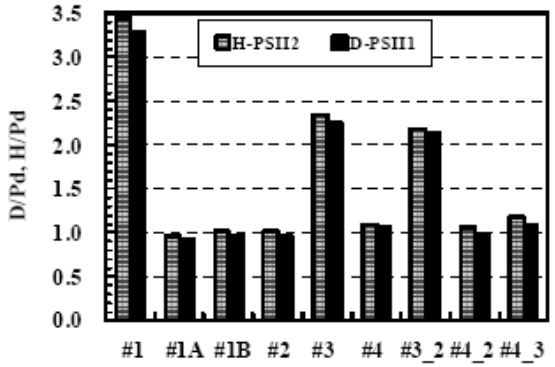

Figure 7. Loading ratio D(H)/Pd for the samples D-PSII1 and H-PSII2.

These results show that the PSII sample can be repeatedly used with little deterioration. The PSII sample serves our purpose.

Next, we discuss time-resolved parameters. The time-resolved specific sorption energy, or differential heat of hydrogen uptake, $\eta_{\mathrm{D(H)}}$, is defined as the output energy per one hydrogen isotope atom absorbed/adsorbed [2];

$$\eta(t) \equiv \frac{\int_t^{t+\Delta t} W_{\mathrm{true}}(t)\mathrm{d}t}{L(t+\Delta t) - L(t)}. \tag{1}$$

The time-variation of $\eta_{\mathrm{D(H)}}$ values is shown in Fig. 8 together with the thermal power evolution in the D-PSII1 and H-PSII2 runs.

Qualitative time-variation of $\eta_{\mathrm{D}}/\eta_{\mathrm{H}}$ values is similar to that for the PZ sample [2]. In the #1 run the first phase is clearly divided into two sub-phases, 1a and 1b. In the 1b-phase both η_{D} and η_{H} values are nearly equal to those for the bulk Pd expressed as the chain lines, while they are extraordinarily large in the 1a-phase. However, the #2 run loses the 1a-phase. And in the #3 absorption run of the oxidized sample, the 1a-phase with the large values of $\eta_{\mathrm{D(H)}} \approx$ 1.0 eV/atom-D(H) is recovered. Using Fig. 11 later, we will discuss $L_{\mathrm{D(H)}}(t) - P_{\mathrm{D(H)}}(t)$ (loading ratio vs. pressure) diagrams to show that the 1b-phase is identified as the phase when only absorption into bulk takes place, and the surface adsorption and/or oxygen pickup reaction could be involved in the 1a-phase.

As for the isotope effect, the value of $\eta_{\mathrm{D}}/\eta_{\mathrm{H}}$ sometimes exceeds unity especially in the beginning of the 1a-phase of the #1 runs, and also in the 1a-phase of the #3 run with a maximum of about 1.3, as is seen in the third graph. In addition, the value of $\eta_{\mathrm{D}}/\eta_{\mathrm{H}}$ sometimes differs from unity also in the 1b-phase. However, $\eta_{\mathrm{D}}/\eta_{\mathrm{H}}$ is erroneous in the 1b-phase, since the change in the loading ratio, the denominator of Eq. (1), is sometimes very small in this phase. It is thought that $\eta_{\mathrm{D}}/\eta_{\mathrm{H}}$ exceeding about 1.1 can hardly be explained solely by chemical isotope effect.

We have changed the extent of oxidization to examine effect of oxygen on hydrogen isotope absorption/adsorption. Figures 9 and 10 show the released heat E_1 and the loading ratio D(H)/Pd, respectively, as a function of the oxidizing fraction x. Here any decrease in the pressure is regarded as an increase in D(H)/Pd.

The lines in the figures show the least-square fittings of the relevant dependencies, where x is the fraction of Pd atoms oxidized as defined above. The parameter D(H)/Pd is the ratio of the number of D(H) atoms used for oxygen pickup and hydridation (absorption and adsorption including spillover effect) to that of the host Pd atoms. We see that D(H)/Pd and E_1 linearly increase with x. As indicated in the figure, the intercepts to the y-axes, or

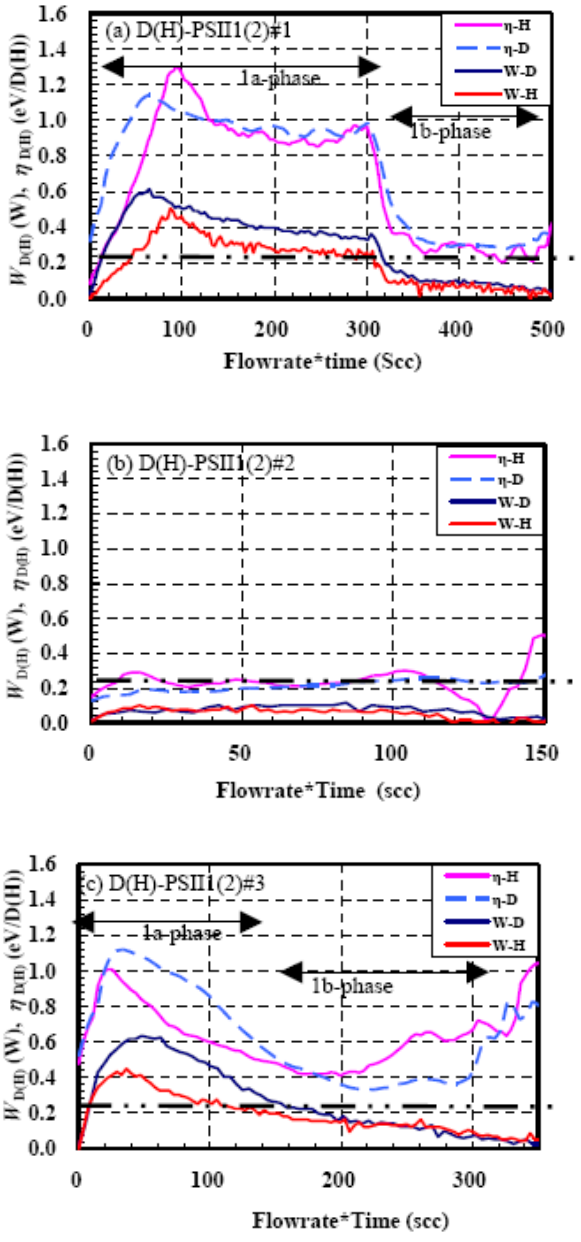

Figure 8. Evolution of heat, W, and the time-dependent absorption energy, η, for D_2 gas and H_2 gas absorption runs D(H)-PSII1(2)#1 (a), D(H)-PSII1(2)#2 (b),.and D(H)-PSII1(2)#3 (c).

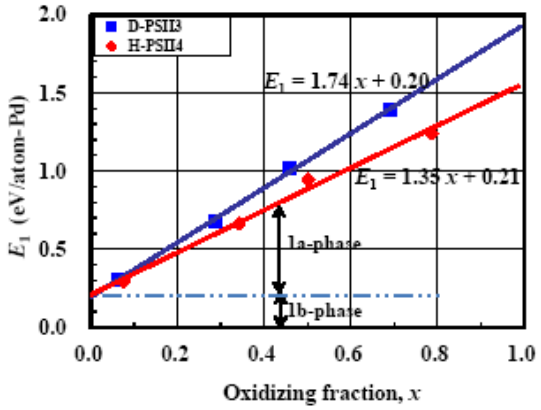

Figure 9. Relation between the specific output energy E_1 and the oxidizing fraction x for the PSII samples.

the values at $x = 0$, correspond to the #2 runs, and therefore to the 1b-phase, while the portions linearly increasing with x correspond to the 1a-phase in which surface adsorption and oxygen pickup take place.

The oxygen pickup reaction from PdO are considered to proceed in the following manner:

$$\mathrm{PdO} + Q_{\mathrm{O}} \rightarrow \mathrm{Pd} + \frac{1}{2}\mathrm{O_2}, \tag{2}$$

$$\mathrm{D(H)_2} + \frac{1}{2}\mathrm{O_2} \rightarrow \mathrm{D(H)_2O} + Q_{\mathrm{wD(H)}}, \tag{3}$$

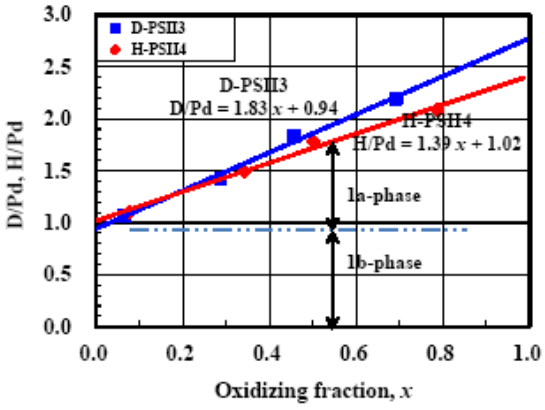

Figure 10. Relation between loading ratio and the oxidizing fraction x for the PSII samples.

where the oxide formation energy $Q_{\mathrm{O}} = 0.886$ eV for the bulky Pd, and the water formation energy $Q_{\mathrm{wD(H)}} = 2.654$ (2.511) eV. Summing up these formulae, we have the following as the oxygen pickup reaction:

$$\mathrm{PdO} + \mathrm{D(H)}_2 \rightarrow \mathrm{Pd} + \mathrm{D(H)}_2\mathrm{O} + Q_{\mathrm{redD(H)}};\ Q_{\mathrm{redD(H)}} = Q_{\mathrm{wD(H)}} - Q_{\mathrm{O}}. \tag{4}$$

For the bulky Pd the oxygen pickup reaction energy $Q_{\mathrm{red\,D(H)}} = 1.768$ (1.625) eV. If hydridation follows the oxygen pickup from PdO with a fraction of x' out of x, we have the following for the output energy $E_{1\mathrm{D(H)}}$;

$$\mathrm{PdO}_x + \left(x' + \frac{y}{2}\right)\mathrm{D(H)}_2 \rightarrow \mathrm{PdO}_{x-x'} + x'\mathrm{D(H)}_2\mathrm{O} + \mathrm{PdD(H)}_y + E_1, \tag{5}$$

$$E_1 = x' Q_{\mathrm{redD(H)}} + y Q_{\mathrm{D(H)}}. \tag{6}$$

Using the above formulae, we can make some discussion under some assumptions.

First, we note that the values of the intercepts to the vertical axes corresponding to the #2 and #4 runs with no oxygen, or the 1b-phase, agree very well to the published absorption energy of 0.2 eV/atom-D(H). From this fact, we can infer that contribution of the surface adsorption should be included in the first term proportional to x'. Namely, the number of hydrogen isotopes adsorbed on the PdO_x surface is considered to be proportional to x.

The water formation does not change the pressure measured with a piezoelectric gauge, as far as the water remains in the gas phase, since H_2O has the same volume as H_2. In this case, the pressure decrease in the 1a-phase is caused by adsorption exclusively. This appears to be the case in the present measurements, as is shown in Fig. 11. Even so, it is difficult to deduce the adsorption energy, since the oxygen pickup also contributes to the first term in Eq. (6).

In contrast, the water molecules could be adsorbed on the sample surface. In this case the water formation yields no volume, and decreases the pressure to be measured as a part of $L_{\mathrm{D(H)}}(t)$. Anyway, it is difficult to separate adsorption and oxygen pickup from each other in the first term in Eq. (6) without further assumption.

Now we discuss $L_{\mathrm{D(H)}}(t) - P_{\mathrm{D(H)}}(t)$ diagrams in comparison to those for another sample to show that the 1b-phase is identified as the phase when only absorption into bulk takes place. Figures 11 and 12 show the time-resolved relation between the loading ratio $L_{\mathrm{D(H)}}(t)$ and the pressure $P_{\mathrm{D(H)}}(t)$ for the PSII and the PNZ2B samples, respectively. The latter is a sample of nanoparticles of Pd·Ni compound dispersed in ZrO_2 prepared by B. Ahern with the melt-spinning method [8]. The hydrogen absorption characteristics of the PNZ2B sample was described partly in Refs. [5,9]. Here we refer only to the $P_{\mathrm{D(H)}}(t) - L_{\mathrm{D(H)}}(t)$ diagram. After hydrogen isotope gas introduction, pressure increases without significant increase in $L_{\mathrm{D(H)}}(t)$ up to about 50 kPa, at which the pressure abruptly decreases down to 7–8 kPa, making a pressure hump. This pressure hump is considered to be typical of supersaturation followed by condensation of the $\mathrm{D(H)}_2\mathrm{O}$ vapor into liquid with a static vapor pressure of about 4 kPa (for H_2O) at room temperature. For the water molecules to condensate, the partial pressure has to exceed more than several times the static vapor pressure to become supersaturation condition.

On the other hand, the pressure hump is not observed in the PSII sample runs. After $L_{\mathrm{D(H)}}(t)$ increases above 1.0, $P_{\mathrm{D(H)}}(t)$ rises above 10(4) kPa with a large isotope effect, which is never related to oxygen pickup reaction, but is common to bulk absorption [2,5]. The former phase with $P_{\mathrm{D(H)}}(t) < 10(4)$ kPa is identified as the 1a-phase with the larger $\eta_{\mathrm{D(H)}}$, and the latter to the 1b-phase with the smaller $\eta_{\mathrm{D(H)}}$ which gives the intercepts to the y-axes in Figs. 9 and 10, or equivalently the lower values of E_1 and D(H)/Pd for oxygen-free runs other than #1 and #3 in Figs. 6 and 7. The isotope effect in the bulk absorption (1b-) phase could be explained by the difference in velocity leading to a difference in probability of tunneling through the periodic potential barriers between the lattice atoms. It is therefore inferred that $D_2O(H_2O)$ formation has negligible effect on the pressure for the present PSII sample.

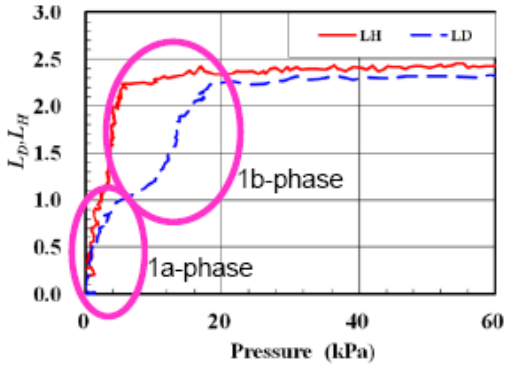

Figure 11. Relation between the loading ratio and the pressure in the D(H)-PSII1(2)#3 runs.

3.2. PNS sample

At the instant of presentation at this conference we did not complete the absorption experiments at elevated temperatures. In the present paper only the room-temperature runs are described.

As mentioned earlier, the isothermal calorimetry has been employed in absorption runs using the PNS samples including the room-temperature runs. Figure 13 shows evolution of the absorption parameters in the room-temperature runs using 10-g aliquots of the PNS sample containing 0.78 g of the Pd_1Ni_6 nanopowders.

We see clearly the sharp 1st-phase peaks of the thermal power output $W_{D(H)}(t)$ with a width of about 35 min, which are coincident with the sharp rising-up of the loading ratio $L_{D(H)}(t)$ to the saturation value of 0.43 (0.39). The powers are integrated to give the specific output energy $E_{1D(H)}$ = 0.51 (0.39) eV/atom-M, where M stands for the metal host atom with the averaged composition of Pd_1Ni_6. These are reevaluated as the energy per one hydrogen isotope atom absorbed to be $Q_{D(H)}$ = 1.2 (1.0) eV/atom-D(H).

The values of $L_{D(H)}(t)$ and $E_{1D(H)}$ are rather modest in comparison with those for the PSII sample. However, if we assume that Ni atoms had no effect on the hydrogen absorption, the values would be seven times larger, which could

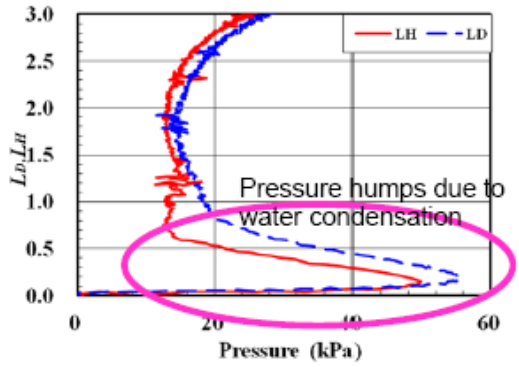

Figure 12. Relation between the loading ratio and the pressure for the PNZ2B samples.

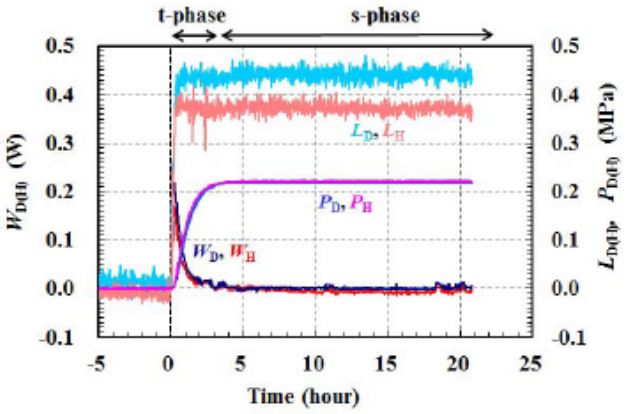

Figure 13. PNS absorption runs at room temperature, D-PNS1#1 and H-PNS2#1. The isothermal calorimetry is used.

be unacceptable. We can conclude therefore that the Pd atom in the present configuration is acting as a catalyzer for hydrogen absorption of Ni nanoparticles.

It is also interesting to note that $Q_{D(H)}$ are comparable to or even larger than those not only for the PSII sample but also for the PNZ2B sample. The potential of the hydrogen absorption sites in the present configuration is comparable to or deeper than in those samples.

The above comparisons with the other samples are tentative, since the different method of calorimetry has been employed for the PNS sample. Further study is needed to confirm the interesting conclusion.

4. Conclusion

The PSII samples have shown distinguishing absorption characteristics summarized in the following:

(1) The as-received PSII samples showed very large loading ratio reaching 3.5 and absorption energy exceeding 2.5 eV/atom-Pd, both being much larger than other Pd nanoparticle samples ever used [2–4].
(2) Subsequent runs without baking and runs after forced de-oxidization showed almost the same characteristics; D(H)/Pd $\approx$ 1.0, and $E_1 \approx$ 0.2–0.3 eV/atom-Pd. These are slightly larger than or equal to those of bulk Pd. However, forced oxidization recovered large values of D(H)/Pd exceeding 2.2 and E_1 exceeding 1.3 eV.
(3) Silica-inclusion of nanoparticles of Pd is effective to make the sample reusable to the hydrogen isotope absorption/adsorption.
(4) The isotope effect in the released heat in the first phase is rather large.

The PNS samples have also shown interesting, though tentative, absorption characteristics:

(1) Pd atoms are acting as a catalyst for hydrogen absorption of Ni nanoparticles.
(2) The potential of the hydrogen absorption sites in the present configuration is comparable to or deeper than in other samples ever tested.

Acknowledgements

The authors thank Dr. Brian Ahern for supplying the PNZ2B sample and valuable discussions. They also appreciate Admatechs Co. Ltd. which provided the silica-included sample.

References

[1] A. Kitamura, T. Nohmi, Y. Sasaki, A. Taniike, A. Takahashi, R. Seto and Y. Fujita, *Phys. Lett.* A **373** (2009) 3109–3112.
[2] A. Kitamura, Y. Miyoshi, A. Taniike, A. Takahashi, R. Seto and Y. Fujita, *J. Condensed Matter Nucl. Sci.* **4** (2011) 56–68.
[3] A. Kitamura, Y. Miyoshi, H. Sakoh, A. Taniike, A. Takahashi, R. Seto and Y. Fujita, *J. Condensed Matter Nucl. Sci.* **5** (2011) 42–51.
[4] H. Sakoh, Y. Miyoshi, A. Taniike, A. Kitamura, A. Takahashi, R. Seto and Y. Fujita, *Proc. 12th Meeting of Japan CF Research Society, JCF12* (2012), pp. 10–18.
[5] Y. Miyoshi, H. Sakoh, A. Taniike, A. Kitamura, A. Takahashi, R. Seto and Y. Fujita, *J. Condensed Matter Nucl. Sci*. **10** (2013) 46–62; A. Takahashi et al., *Session of New Energy Technology, 241st ASC National Meeting*, Mar. 2011.
[6] H. Sakoh, Y. Miyoshi, A. Taniike, A. Kitamura, A. Takahashi, R. Seto and Y. Fujita, 17th *Int. Conf. Condensed Matter Nucl. Sci*., Daejeon, Korea, Aug. 2012.
[7] D. A. Kidwell, A. E. Rogers, K. Grabowski and D. Knies, 17th *Int. Conf. Condensed Matter Nucl. Sci*., ENEA, Rome, Italy, 2009.
[8] B. Ahern, Private communication.
[9] A. Takahashi, A. Kitamura, Y. Miyoshi, H. Sakoh, A. Taniike, R. Seto and Y. Fujita, *ICCF16*.
[10] R. Laesser and K. H, Klatt, *Phys. Rev*. **B28** (1983)748–758.